



# The linkage between stratospheric water vapor and surface temperature in an observation-constrained coupled general circulation model

Yuan Wang<sup>1</sup> · Hui Su<sup>1</sup> · Jonathan H. Jiang<sup>1</sup> · Nathaniel J. Livesey<sup>1</sup> · Michelle L. Santee<sup>1</sup> · Lucien Froidevaux<sup>1</sup> · William G. Read<sup>1</sup> · John Anderson<sup>2</sup>

Received: 12 December 2015 / Accepted: 7 June 2016 / Published online: 13 June 2016  
© Springer-Verlag Berlin Heidelberg 2016

**Abstract** We assess the interactions between stratospheric water vapor (SWV) and surface temperature during the past two decades using satellite observations and the Community Earth System Model (CESM). From 1992 to 2013, to first order, the observed SWV exhibited three distinct piece-wise trends: a steady increase from 1992 to 2000, an abrupt drop from 2000 to 2004, and a gradual recovery after 2004, while the global-mean surface temperature experienced a strong increase until 2000 and a warming hiatus after 2000. The atmosphere-only CESM shows that the seasonal variation of tropical-mean ( $30^{\circ}\text{S}$ – $30^{\circ}\text{N}$ ) SWV is anticorrelated with that of the tropical-mean sea surface temperature (SST), while the correlation between the tropical SWV and SST anomalies on the interannual time scale is rather weak. By nudging the modeled SWV to prescribed profiles in coupled atmosphere-slab ocean experiments, we investigate the impact of SWV variations on surface temperature change. We find that a uniform 1 ppmv (0.5 ppmv) SWV increase (decrease) leads to an equilibrium global mean surface warming (cooling) of  $0.12 \pm 0.05^{\circ}\text{C}$  ( $-0.07 \pm 0.05^{\circ}\text{C}$ ). Sensitivity experiments show that the equilibrium response of global mean surface temperature to SWV perturbations over the extratropics is larger than that over the tropics. The observed sudden drop of SWV from 2000 to 2004 produces a global mean surface cooling of about  $-0.048 \pm 0.041^{\circ}\text{C}$ , which suggests that a persistent change in SWV would make an imprint on long-term

variations of global-mean surface temperature. A constant linear increase in SWV based on the satellite-observed rate of SWV change yields a global mean surface warming of  $0.03 \pm 0.01^{\circ}\text{C}/\text{decade}$  over a 50-year period, which accounts for about 19 % of the observed surface temperature increase prior to the warming hiatus. In the same experiment, trend analyses during different periods reveal a multi-year adjustment of surface temperature before the response to SWV forcing becomes strong relative to the internal variability in the model.

**Keywords** Stratospheric water vapor · Global warming · General circulation model · Radiative forcing and feedbacks

## 1 Introduction

Global mean surface temperature warmed by about  $0.12^{\circ}\text{C}/\text{decade}$  from the 1950s to the turn of the century, most likely attributable to significant increases in anthropogenic carbon dioxide and other greenhouse gases (IPCC 2013). However, the steady increase in global surface temperature has almost vanished since 2000 (Kaufmann et al. 2011). The question of whether such a hiatus in global warming is caused by external forcings (such as volcanic eruptions) or internal variabilities (such as the Pacific Decadal Oscillation or Atlantic Multi-decadal Oscillation) in the atmosphere–ocean system is still under debate (Meehl et al. 2011; Kosaka and Xie 2013; Booth et al. 2012; Trenberth and Fasullo 2013; Watanabe et al. 2014; England et al. 2014; Chen and Tung 2014). As an important greenhouse gas, water vapor has great potential to modulate global climate by altering the infrared opacity of the atmosphere (e.g., Soden and Held 2006). In particular,

✉ Yuan Wang  
yuan.wang@jpl.nasa.gov

<sup>1</sup> Jet Propulsion Laboratory, California Institute of Technology, Pasadena, CA 91109, USA

<sup>2</sup> Department of Atmospheric and Space Sciences, Hampton University, Hampton, VA 23668, USA

stratospheric water vapor (SWV) provides about +0.3 W/(m<sup>2</sup> K) climate feedback to global warming (Dessler et al. 2013), in accordance with the time-varying stratospheric radiative effect averaged over multiple climate models (Huang 2013). In contrast to well-mixed greenhouse gases, SWV exhibits large inhomogeneity in its spatial distribution and has large temporal variations. Previous studies (Rosenlof et al. 2001; Solomon et al. 2010) reported a 1%/year increase of water vapor in the middle stratosphere from the 1950s to 2000, followed by a sudden decrease of water vapor in the lower stratosphere by 10 % from 2000 to 2004, based on satellite and balloon measurements. Variations of SWV are closely linked with the temperature and circulation patterns in the lower stratosphere. Randel et al. (2006) showed that SWV and tropical tropopause temperature are highly correlated, both being regulated by the tropical upwelling as part of the Brewer-Dobson Circulation (BDC). Rosenlof and Reid (2008) showed that observed SWV and sea surface temperature (SST) are correlated over the tropical warm pool region. Dessler et al. (2013) further discussed the relative importance of the BDC, tropical temperature and the Quasi-Biennial Oscillation (QBO) in regulating SWV abundances and identified relatively larger roles for the BDC and tropical temperature than for the QBO. Moreover, when these three factors act in phase, large variations of SWV can be detected (Dessler et al. 2013).

Radiative forcing associated with SWV changes has been quantified using different radiation kernels (e.g. Forster et al. 2001). Solomon et al. (2010) examined the dependence of surface radiative forcing on the vertical distribution of SWV, illustrating that water vapor near the tropopause exerts the largest radiative forcing on the surface, about 0.03 W/m<sup>2</sup>/ppmv/km. Gilford et al. (2016) estimated that the lower SWV concentrations in the period of 2005–2013, compared to the 1990s, would produce a radiative forcing around −0.045 W/m<sup>2</sup>, about 12 % of the magnitude of the concurrent greenhouse gas warming by CO<sub>2</sub>. Sensitivity of estimated radiative forcing to the representation of SWV in radiation codes has been discussed (Forster et al. 2001), and differences of up to 96 % in SWV adjusted radiative forcing between different radiative codes were reported by a comparative study (Maycock and Shine 2012). The radiative impacts of SWV variations have been assessed using different models with varying degrees of sophistication. Maycock et al. (2013) simulated the atmospheric response to idealized changes in SWV using a vertically extended atmosphere model and concluded that long-term increases in SWV may cool stratospheric temperature, enhance the BDC, and even induce a poleward shift of storm tracks. Using an Earth system Model of Intermediate Complexity (EMIC) with simplified dynamical framework and physics parameterizations,

Solomon et al. (2010) reported that the feedback from SWV enhanced the decadal global surface warming rate by 30 % from 1980 to 2000, and further suggested that the sudden decrease of SWV after 2000 slowed down the rate of global surface warming by 25 %. As the SWV and surface temperature interactions involve complex feedbacks from tropospheric water vapor, clouds and the large-scale circulation, it is not clear whether such EMIC simulation results are comparable to those from fully coupled atmosphere–ocean models.

Comprehensive atmosphere–ocean coupled general circulation models (AOGCMs) have been widely used to assess the transient and equilibrium responses of the climate system to forcing agents like carbon dioxide (Held et al. 2010; Geoffroy et al. 2013). However, the responses to SWV variations in AOGCMs remain to be explored. The primary objective of this study is to investigate the influence of SWV on surface temperature using a state-of-the-art AOGCM in conjunction with a multi-year record of satellite-based SWV observations. We focus on the period for which merged satellite records are currently available, i.e., from 1991 to 2013.

The observations used in this paper are described in Sect. 2. The model and an atmosphere-only experiment, driven by observed SST, are presented in Sect. 3.1. Section 3.2 shows equilibrium and transient responses of surface temperature to SWV perturbations using the atmosphere-slab ocean coupled model. Conclusions and discussions are provided in Sect. 4.

## 2 Observed SWV and surface temperature variations

Water vapor fields from the Global Ozone Chemistry and Related trace gas Data records for the Stratosphere (GOZCARDS) project from 1992 to 2013 are used to characterize the observed interannual variations of SWV and to provide a constraint on SWV in AOGCM simulations. The GOZCARDS water vapor dataset (Anderson et al. 2013; Froidevaux et al. 2015) combines monthly zonal mean satellite-derived global stratospheric composition measurements from the HALOgen Occultation Experiment (HALOE) and the Microwave Limb Sounder (MLS) on the Upper Atmosphere Research Satellite (UARS), the Atmospheric Chemistry Experiment Fourier Transform Spectrometer (ACE-FTS), and the MLS on Aura. As shown in Fig. 1a, water vapor in the upper troposphere and lower stratosphere (150–50 hPa) has exhibited dramatic variations during the past two decades. Around the year 2000, there was a rapid and significant decrease of SWV, which has been attributed to an increase in the mean tropical upwelling and decrease in tropopause temperature

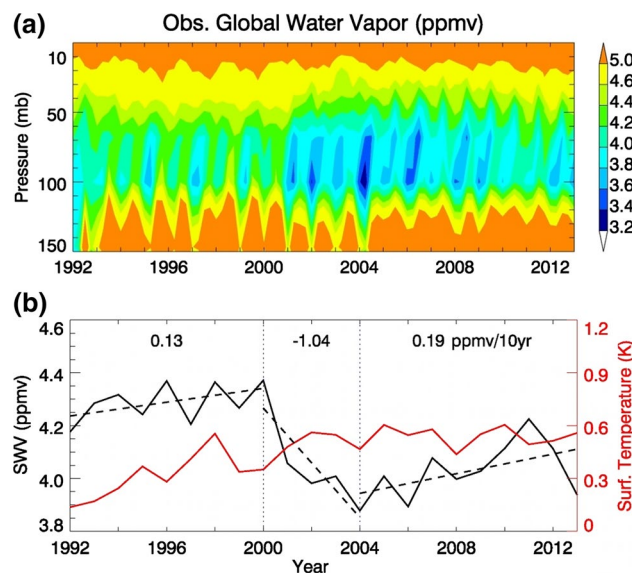


**Fig. 1** Observed temporal evolution of global-mean stratospheric water vapor over 1992–2013 from the GOZCARDS dataset. **a** Seasonal mean SWV at all levels in the lower and middle stratosphere. **b** Annual mean SWV averaged between 45 and 100 hPa. *Solid black lines* denote observations; *dashed black lines* denote the linear regressions. The combined surface temperature anomalies from the CRU and GISS observational datasets are overlaid in red

associated with the strengthening of the BDC (Randel et al. 2006). After the abrupt change from 2000 to 2004, SWV has slowly increased but has not yet returned to the pre-2000 amount, thus resulting in lower decadal-mean SWV in the period after 2000 compared to that in the 1990s. The smoother seasonal variation after 2004 in water vapor below 100 hPa results from the higher-temporal-resolution measurements by Aura MLS compared to the pre-2004 period.

The characteristic temporal variations of SWV can be represented by water vapor over the 45–100 hPa layer, showing three distinct piece-wise trends over the study period (Fig. 1b): an increasing trend from 1992 to 2000, a sudden drop from 2000 to 2004, and another increasing trend after 2004. Another significant drop in SWV occurred after 2011 (Urban et al. 2014; Froidevaux et al. 2015; Gilford et al. 2016). However, given its weaker magnitude than the 2000–2004 drop, we do not single this one out in our study. Linear regression fits yield 0.13, −1.04 and 0.19 ppmv/decade rates of change in global SWV averaged between 45 hPa and 100 hPa, respectively, for these three periods. The trend analyses based on GOZCARDS should be free of the patching problems arising from the disparities between different instruments mentioned by Heglín et al. (2014), because the same instruments were used to measure SWV within each period, e.g. HALOE and UARS MLS from 1992 to 2004 and Aura MLS and ACE-FTS after 2004.

The observed variation of the anomaly in global mean surface temperature from the combined Climatic Research Unit (CRU, Morice et al. 2012) and NASA GISS (Hansen et al. 2010) datasets is shown in Fig. 1b. In contrast with the three distinct trends of SWV, surface temperature shows a steady increase from 1992 to 2000 and no significant trends after 2000. The observed tropical mean surface temperature (not shown) exhibits similar interannual variations, i.e. an increasing trend before 1999 and no significant trend after 2000. The lack of a clear relationship between SWV and surface temperature based on these observations makes it important to use an atmosphere–ocean coupled model to assess the interactions between SWV and surface temperature.

### 3 GCM simulations

The NCAR Community Earth System Model (CESM) version 1.2.1 is employed in this study. Two types of model setup are adopted. One uses only the atmosphere component of CESM, i.e. the Community Atmosphere Model, Version 5 (CAM5), driven by observed SST. The other model setup couples CAM5 with a mixed-layer slab ocean model (SOM), with all external forcings (i.e., solar flux, volcanoes, greenhouse gases and aerosols) fixed to a year 2000 scenario. The ocean horizontal heat transport fluxes and deep-water heat exchange (Q-fluxes) at each grid point in SOM are prescribed using the monthly mean climatology from CESM fully coupled simulations (Hurrell et al. 2013). Such a CAM-SOM setup is useful for examining climate responses to certain forcings by assuming no modulation of the ocean circulation. The AGCM coupled to SOM has been widely used to examine climate feedbacks and climate change in many previous studies (e.g., Meehl et al. 2000; Gregory and Webb 2008). The CAM5 horizontal resolution is 1.9° in latitude and 2.1° in longitude. Ten out of the 30 vertical levels are located in the stratosphere, with the model top at 3.6 hPa.

#### 3.1 Simulations forced by observed SST

One important aspect of the relationship between surface temperature and SWV is the response of SWV to the interannual variation of SST. Su et al. (2006) and Jiang et al. (2010) reported that tropical-mean upper troposphere water vapor and SST are closely correlated at the interannual time scale during the Aura MLS observation period from 2004 to 2009. We investigate SWV responses to SST in the CAM5 model driven by observed SST from 1990 to 2005, with all other external forcings fixed. A correlation analysis over the 16-year period (1990–2005) in Fig. 2a shows that the simulated tropical SWV (30°S–30°N) at 88 hPa is anti-correlated

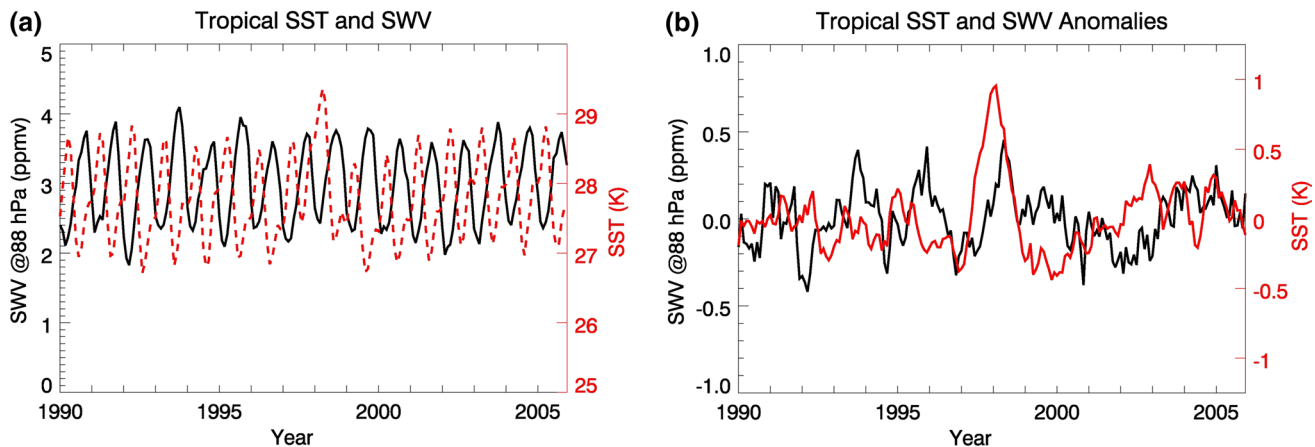


**Fig. 2** **a** SWV (in black) over  $30^{\circ}\text{S}$ – $30^{\circ}\text{N}$  at 88 hPa simulated by CAM5 with time-varying observed SST and central tropical ( $10^{\circ}\text{S}$ – $10^{\circ}\text{N}$ ) SST (in red). **b** The same as (a) but anomalies of SWV and SST relative to the monthly climatology, such that seasonal variability is subtracted out

with the prescribed tropical SST ( $10^{\circ}\text{S}$ – $10^{\circ}\text{N}$ ) with the correlation -0.67. To examine the SST impact on SWV on the interannual scale, we show the simulated tropical SWV anomalies ( $30^{\circ}\text{S}$ – $30^{\circ}\text{N}$ ) at 88 hPa and the prescribed tropical SST anomalies ( $10^{\circ}\text{S}$ – $10^{\circ}\text{N}$ ) relative to the mean seasonal cycle in Fig. 2b. A correlation analysis with different temporal lags reveals that the maximum correlation between the tropical-mean SST and SWV anomalies is only 0.36 at a half-year lag (SST leading SWV). The correlations between SWV and SST anomalies are always weak (less than 0.4) no matter which regions (tropics, extratropics or the Western Pacific warm pool) are chosen for analysis (table not shown). Moreover, the observed sudden drop of SWV from 2000 to 2004 is not fully reproduced in the CAM5 simulation driven by observed SST. The weak correlation between the tropical SST and SWV on the interannual scale suggests that tropical SST is not the sole driver for the interannual variations of SWV. Other factors such as the BDC and QBO are also at work (Liang et al. 2011; Dessler et al. 2013, 2014). For example, Randel et al. (2004) suggested that interannual changes in SWV are well correlated with anomalies in tropical tropopause temperatures that are associated with the QBO and El Niño–Southern Oscillation (ENSO). Based on observational data, Liang et al. (2011) also found that the modes of ENSO and QBO both affect the interannual variability of tropical SWV. Castanheira et al. (2012) suggested that the sudden decrease in SWV after 2000 is closely linked to a step-like increase in the tropical upwelling that may not be captured in the current CESM. We note that there are large uncertainties associated with the model-simulated BDC, convective overshooting and isentropic mixing, particularly given the model's coarse vertical resolution and parameterized deep convection (Richter et al. 2014). In addition, the QBO is not well represented in the current CESM.

### 3.2 Coupled atmosphere–ocean simulations with a nudging approach

Results from the 50-year CESM free run using CAM5 coupled with a slab-ocean model have been evaluated against a number of observations. The simulated clear-sky outgoing longwave radiation (OLR) agrees well with that from the Clouds and the Earth's Radiant Energy System (CERES) measurements (Fig. 3a, b). The global-mean clear-sky OLR difference between the model and the CERES observation is  $-3.2 \text{ W/m}^2$ , corresponding to a  $-1.2\%$  bias. The simulated spatial patterns and magnitude of global SST are in good agreement with the merged Hadley Optimal Interpolation SST observations (Hurrell et al. 2008) (Fig. 3c, d). Comparisons of tropical air temperature vertical profiles from the model simulations with observations from the Atmospheric Infrared Sounder (AIRS) and the European Centre for Medium-Range Weather Forecasts (ECMWF) reanalysis (Fig. 4) show that CESM generally reproduces the vertical variations of temperature below 100 hPa and captures the height of the tropical tropopause as indicated by the coldest temperature point, but underestimates the temperature in the stratosphere. The tropical surface temperature in the model is 3–4 K higher than observed, presumably due to unrealistic air-sea interactions over certain tropical regions, such as the Eastern Pacific, in the coupled model, as shown in Fig. 3d.

Comparison of SWV between CESM and MLS climatology in Fig. 5 shows that the model underestimates the water vapor amount in the lower stratosphere by 10–20 %, corresponding to 0.4–0.8 ppmv difference, and such biases are much smaller than those in the upper troposphere and in the extratropical middle stratosphere. The model underestimates the water vapor in the middle stratosphere by up to 50 %, likely due to the simple treatment of the water vapor

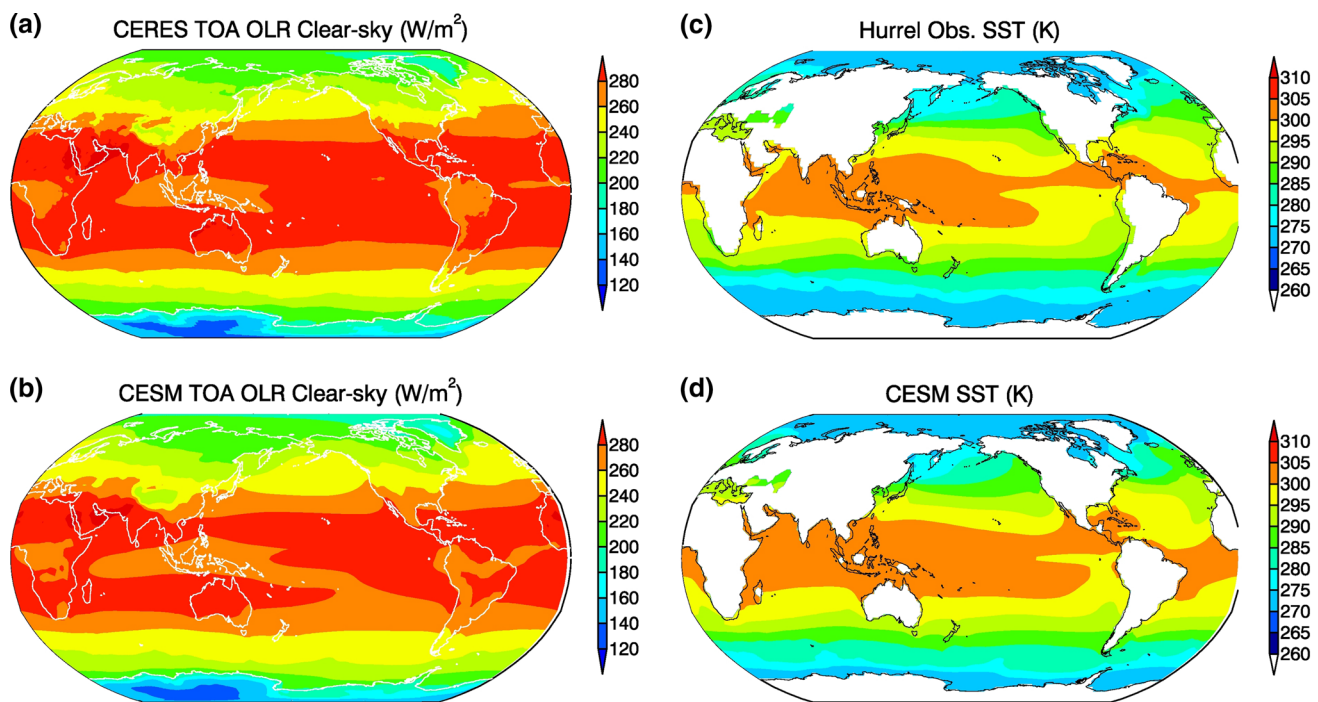


**Fig. 3** **a** observed clear-sky and top-of-atmosphere (TOA) outgoing longwave radiation flux (OLR) from CERES satellite measurements, **b** CESM simulated climatology of clear-sky OLR, **c** the observed

SST climatology from the merged Hadley-OI SST observations, and **d** CESM simulated SST climatology

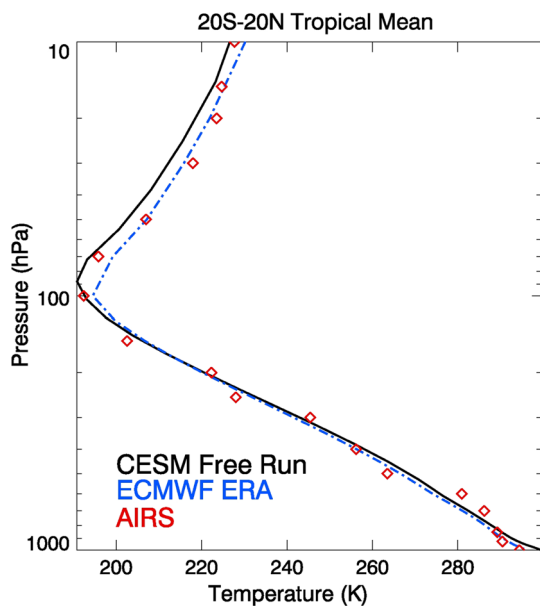


**Fig. 4** Comparison of air temperature profiles over the tropics from AIRS satellite measurements, ECMWF Interim reanalysis data (ERA-I) and the CESM free run

source from methane oxidation. In addition, the model largely overestimates water vapor in the upper troposphere (UTWV), owing to inadequate representation of the processes that control the variability of UTWV, such as deep

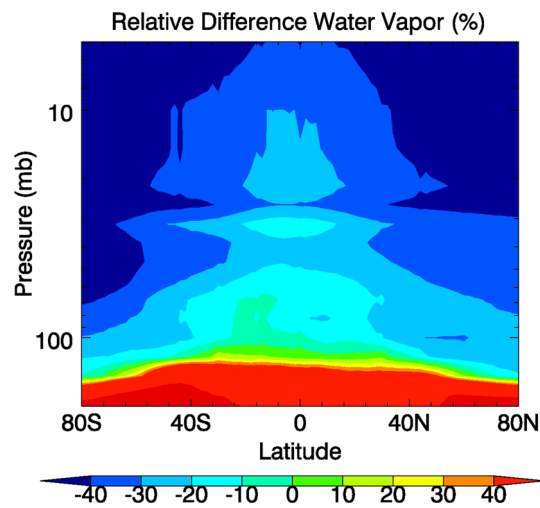


**Fig. 5** Percentage differences of zonal mean SWV between MLS measurements and the CESM free run, defined as  $100 \times (\text{model} - \text{obs.})/\text{obs.}$

convection. Similar UTWV biases were found in most of the climate models in the Coupled Model Inter-comparison Project Phase 5 (CMIP5) (Jiang et al. 2012; Takahashi et al. 2015), as well as in reanalysis datasets (Jiang et al. 2015).

To conduct sensitivity experiments using perturbed SWV, we employ a nudging approach to manipulate the simulated water vapor in the stratosphere, in a similar way to Zhang

**Table 1** Numerical experiment design

Experiment name	Experiment description	Integration years	Ensemble runs
Exp. 1	CAM5 with time-varying SST	16	2
Exp. 2	CESM with 1 ppmv SWV increase	70	4
Exp. 3	CESM with 0.5 ppmv SWV decrease	70	4
Exp. 4	CESM with 0.5 ppmv SWV decrease over tropics	70	4
Exp. 5	CESM with 0.5 ppmv SWV decrease over extratropics	70	4
Exp. 6	CESM with the year 2000 SWV sudden drop	70	4
Exp. 7	CESM with a linear SWV increase rate	50	4

et al. (2014). A tendency term is added in the water vapor prognostic equation with an adjustable time constant  $\tau$  according to:

$$\frac{\partial q_v}{\partial t} = \left( \frac{\partial q_v}{\partial t} \right)_{physics} + \left( \frac{\partial q_v}{\partial t} \right)_{chemistry} + \dots + \frac{\bar{Q}_v + P - q_v}{\tau}, \quad (1)$$

where  $\bar{Q}_v$  is the monthly-mean SWV at each grid point from the CESM 50-yr climatology and  $P$  is the SWV perturbation prescribed as a constant or from satellite observations. For all control runs,  $P$  is equal to zero. Such nudging is performed for the stratosphere only above the model tropopause height diagnosed from modeled temperature vertical lapse rates (Reichler et al. 2003). In order to adjust water vapor to a monthly climatology, we choose  $\tau = 1$  day. Using this nudging framework we can control the modeled SWV amount and its spatial and temporal variations in order to assess the impacts of SWV variations on surface temperature while minimizing the feedback from changing surface temperature on SWV. Considering that ocean heat transport Q-fluxes in the SOM are prescribed using the monthly climatology from the CESM fully coupled simulations, we choose to nudge the SWV towards the model monthly climatology rather than the MLS monthly climatology at each grid cell of CESM (Zhang et al. 2014). Note that since the fluxes and heat exchange are prescribed in our experiments, the SWV forcing will not induce any modulation on the ocean circulations. Before doing any sensitivity experiments, we perform a 50-yr CESM run with the climatological SWV to allow the atmosphere–ocean coupler to spin up. Ensemble simulations are carried out with random perturbations in the initial temperature field to achieve statistical robustness of the results. Each experiment consists of four ensemble runs for both control and sensitivity cases (Table 1).

### 3.2.1 Long-term equilibrium response to constant SWV perturbations

In a set of perturbation runs, we elevate SWV by 1 ppmv uniformly at all levels in the stratosphere (Exp. 2). The

simulations are integrated for 70 years after the perturbations are imposed, and the average for the last 50 years is calculated. Under a constant forcing of a 1 ppmv increase in SWV, the model produces a 0.12 °C increase in global-mean surface temperature with a standard deviation of 0.05 °C among the four ensemble members. Note that the surface temperature increase induced by SWV is not uniform over the globe (Fig. 6a). This warming inhomogeneity is caused by the modifications to the general circulation and by the nonlinear response in different regions of the globe. The surface downwelling longwave radiative flux in clear-sky conditions increases by 0.91 W/m<sup>2</sup> in global mean. The spatial pattern of the all-sky downward LW flux (not shown here) is quite similar to that of the clear-sky downward LW flux. The reason we only show the clear-sky fluxes is that we want to emphasize that changes in temperature are mainly caused by changes in water vapor amount, rather than changes in cloud amount. Figure 6a, b show that the spatial pattern of surface temperature change is mostly consistent with that of clear-sky downwelling longwave radiation at the surface, indicating that the surface warming is to some extent a consequence of the enhanced greenhouse effect of SWV. In spite of the agreement in spatial patterns between the surface forcing and temperature change, the contrast of different temperature sensitivities between the tropics and polar regions is still evident. A relatively large increase in surface radiative forcing (greater than 1.2 W/m<sup>2</sup>) in the tropics does not result in temperature changes larger than 0.2 °C, whereas a moderate increase in surface radiative forcing (less than 1.2 W/m<sup>2</sup>) in the polar regions induces significant temperature increases of up to 0.5 °C. Such a high sensitivity of surface temperature at high latitudes is mainly attributed to the positive albedo feedback from sea ice changes.

Considered simplistically, assuming that the average lower stratospheric water vapor amount is about 4 ppmv, with a 10 %/decade increasing trend from 1980 to 2000 based on balloon measurements (Rosenlof et al. 2001), the CESM equilibrium response above would imply a global surface warming rate of about 0.048 °C/decade over the same period. Such a warming rate corresponds to about

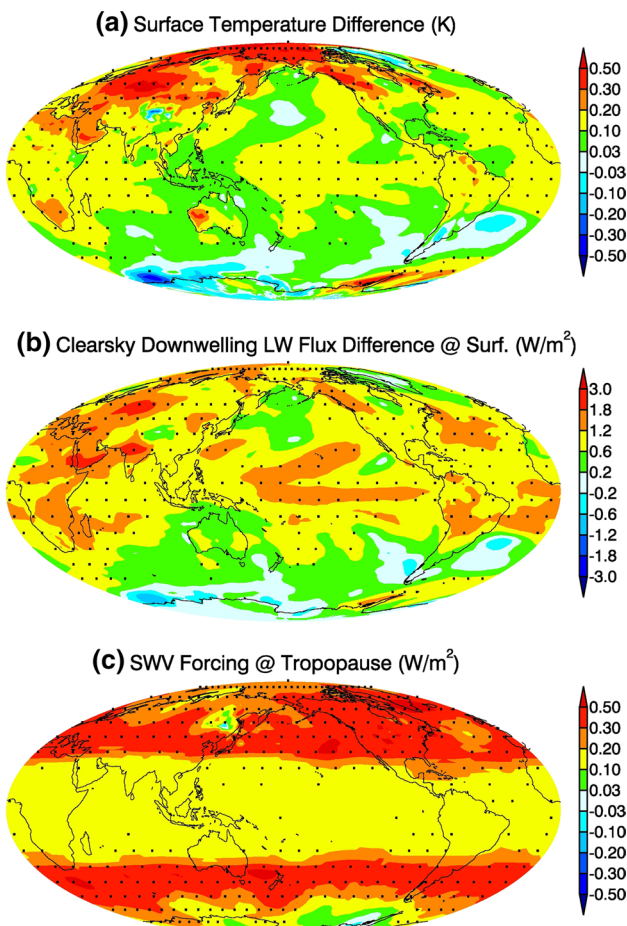


**Fig. 6** CESM simulated equilibrium responses of: **a** surface temperature, **b** surface downwelling longwave radiation flux in clear-sky, and **c** SWV forcing represented by the change in downwelling longwave radiation flux at the tropopause due to a uniform 1 ppmv increase in SWV. Dots indicate the 95 % significance level in a Student's *t* test

28 % of the observed decadal surface temperature increase ( $0.17^{\circ}\text{C}/\text{decade}$ ) from 1980 to 2000. This estimate is close to the 30 % contribution of SWV to the global-mean surface warming suggested by Solomon et al. (2010).

We also diagnose the radiative forcing of SWV based on the model radiation fluxes output at the tropopause level, as done in previous studies (Forster et al. 2001; Maycock and Shine, 2012). By calculating the difference of downwelling longwave radiation fluxes at the tropopause after the temperature adjustment (Fig. 6c), the longwave radiative forcing of a 1 ppmv increase in SWV is  $0.23 \text{ W/m}^2$  in the global mean, consistent with previous radiation kernel calculations of direct SWV forcing after a stratospheric adjustment, namely about  $0.24 \text{ W/m}^2/\text{ppmv}$  at the tropopause (Solomon et al. 2010; Dessler et al. 2013). This forcing comparison confirms that the NCAR CESM provides a reasonable radiation calculation compared to other model experiments. Comparing Fig. 6b, c, the clear differences

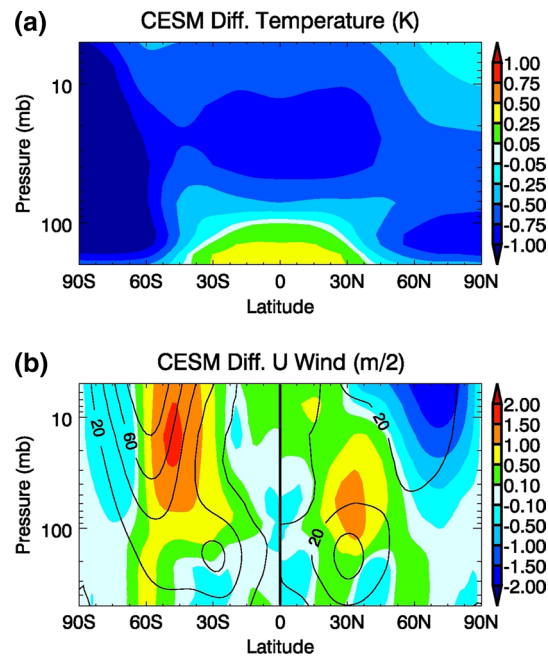


**Fig. 7** CESM simulated equilibrium responses of: **a** air temperature and **b** zonal wind to a uniform 1 ppmv increase in SWV. In **(b)**, the Southern Hemisphere shows changes in the monthly mean zonal wind in July, and the Northern Hemisphere shows changes in the monthly mean zonal wind in January. Contour lines indicate monthly climatological mean zonal wind in the control experiment

between the tropopause and surface patterns of SWV longwave radiative forcing indicate the role of the troposphere in regulating the radiative fluxes. The global SWV increase induces the most significant stratospheric temperature reduction over the Antarctic (Fig. 7a), primarily due to the strengthened stratospheric polar vortex there. The location and strength of the polar vortex can be identified by the wintertime zonal winds in the stratosphere. Figure 7b shows a stronger and expanded winter polar vortex only over Antarctica in response to the SWV increase, which may provide a feedback to reduce the stratospheric temperature. Such a dramatic adjustment masks the regional SWV radiative forcing and explains the insignificant surface responses over the Antarctic (Fig. 6a, b).

By contrast, if we decrease SWV uniformly by 0.5 ppmv over the globe at all levels in the stratosphere (Exp. 3), the long-term response of the global-mean surface temperature is  $-0.072^{\circ}\text{C}$  ( $\pm 0.048^{\circ}\text{C}$ ), with a spatial pattern similar to that of the clear-sky downwelling longwave radiative flux change ( $-0.52 \text{ W/m}^2$ ) at the surface (Fig. 8a, b). The “polar amplification” phenomenon also occurs in this experiment. Considering that the magnitude of surface temperature changes in Exp. 3 ( $0.072^{\circ}\text{C}$ ) is larger than half of that in Exp. 2 ( $0.12^{\circ}\text{C}$ ), we conclude that the response of surface temperature to SWV is not strictly linear because of nonlinear feedbacks in the troposphere. The adjusted radiative

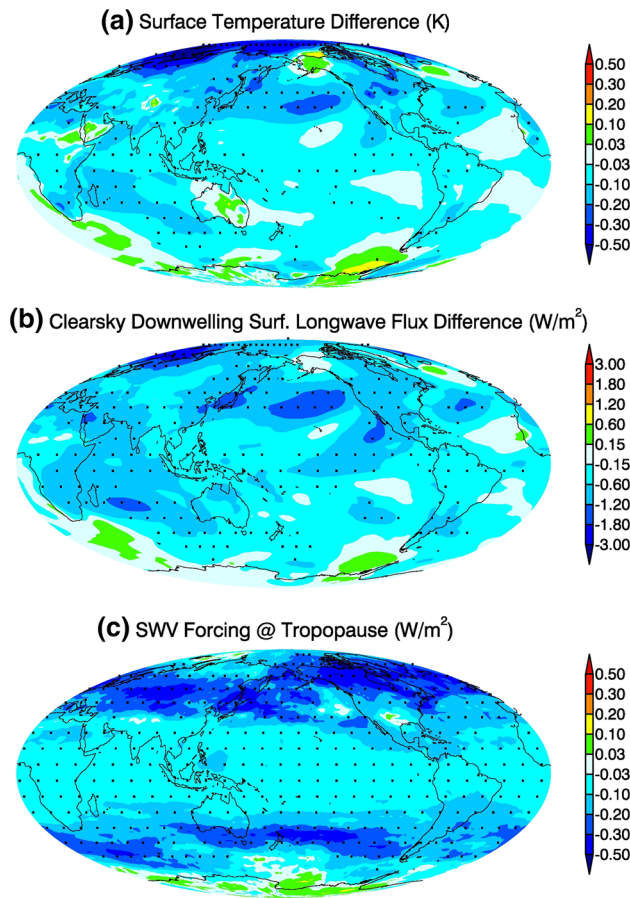


**Fig. 8** As Fig. 6 but for the experiment with a uniform 0.5 ppmv decrease in SWV

forcing of SWV at the tropopause is also found not to be simply proportional to the SWV amount, since the forcing in Exp. 3 is  $-0.16 \text{ W/m}^2$ , larger than half of the  $0.23 \text{ W/m}^2$  in Exp. 2. Part of the nonlinearity of the surface response could also stem from the fact that these simulations only consist of limited ensemble members. As shown in Deser et al. (2010), a large number of ensemble members (e.g. more than twenty) may be needed to obtain a robust pattern for a given forcing.

Note that SWV radiative forcing at the tropopause in both Exp. 2 and 3 is larger over the extratropical regions ( $90^\circ\text{S}$ – $30^\circ\text{S}$ ,  $30^\circ\text{N}$ – $90^\circ\text{N}$ ) than over the tropics ( $30^\circ\text{S}$ – $30^\circ\text{N}$ ), presumably as a result of the lower tropopause height in the extratropics. Hence, water vapor variations below the 80 hPa level (the typical tropical tropopause height) over the extratropics provide extra radiative forcing compared to those over the tropics. This is consistent with Dessler et al. (2013), who noted that one-third of the positive feedback of SWV is attributed to increases in tropical SWV, with the remaining two-thirds attributed to increases in extratropical SWV.

### 3.2.2 SWV perturbation at different latitudes and the sudden drop near 2000

We perform additional experiments to examine the latitude dependence of SWV forcing and surface temperature response. In Exp. 4, SWV is decreased by 0.5 ppmv only over the tropics, and SWV over other latitudes is held constant (Fig. 9a). As shown in Fig. 9b, the surface temperature shows insignificant changes in the tropics, while there is discernable cooling (warming) over the Arctic (Antarctic). Again, the distinctive responses over the two poles are attributed to the different stratospheric temperature adjustments. The global mean temperature change is insignificant, as it is equal to  $0.001^\circ\text{C}$  with a standard deviation of  $0.083^\circ\text{C}$ . In contrast, a uniform 0.5 ppmv SWV decrease only over the extratropics in Exp. 5 (Fig. 9c) leads to a significant global average cooling of  $-0.062^\circ\text{C}$  ( $\pm 0.041^\circ\text{C}$ ). These sensitivity experiments suggest that variations of SWV at middle or higher latitudes exert a larger influence on the global radiation budget and play a greater role in surface temperature change than SWV variations of the same magnitude over the tropics. Similar spatial dependencies of a certain type of radiative forcing have been reported in previous model studies (i.e., Hansen et al. 1997; Wang et al. 2015).

The GOZCARDS dataset shows that the abrupt reduction of water vapor after 2000 mainly occurred between 50 and 200 hPa. From the zonal mean patterns of the SWV difference between 2001–2004 and 1997–2000 in Fig. 9e, the mid-latitudes experienced a 0.2–0.3 ppmv decrease in SWV, whereas the largest SWV drop (greater than 0.5 ppmv) occurred over the low-latitude region ( $30^\circ\text{S}$ – $30^\circ\text{N}$ ). SWV at levels above 30 hPa even increased to varying degrees near the polar regions, but the radiative influence of these levels on surface temperature is limited. We impose such observed SWV changes from 1997 to 2004 as a constant perturbation in the model for 70 years (Exp. 6). The equilibrium response of the surface temperature is about  $-0.048^\circ\text{C}$  ( $\pm 0.041^\circ\text{C}$ ) in the global mean. If we assume that such a temperature decrease occurs within the 8 years from 1997 to 2004, then the linearized cooling rate is  $-0.060^\circ\text{C}/\text{decade}$ . The magnitude of the surface temperature cooling rate due to the SWV reduction is about one third of the observed global warming rate ( $0.17^\circ\text{C}/\text{decade}$ ) from 1980 to 2000. Such an estimated contribution of the SWV sudden drop near 2000 to the slowdown of the global warming rate is comparable to the previous assessment by Solomon et al. (2010), who reported about a 25 % contribution.

The ensemble mean of the adjusted radiative forcing at the tropopause due to the abrupt drop in water vapor is about  $-0.094 \text{ W/m}^2$  in the global mean, which is consistent with the radiation transfer calculation of about  $-0.098 \text{ W/m}^2$  using a line-by-line radiative model (Solomon et al.

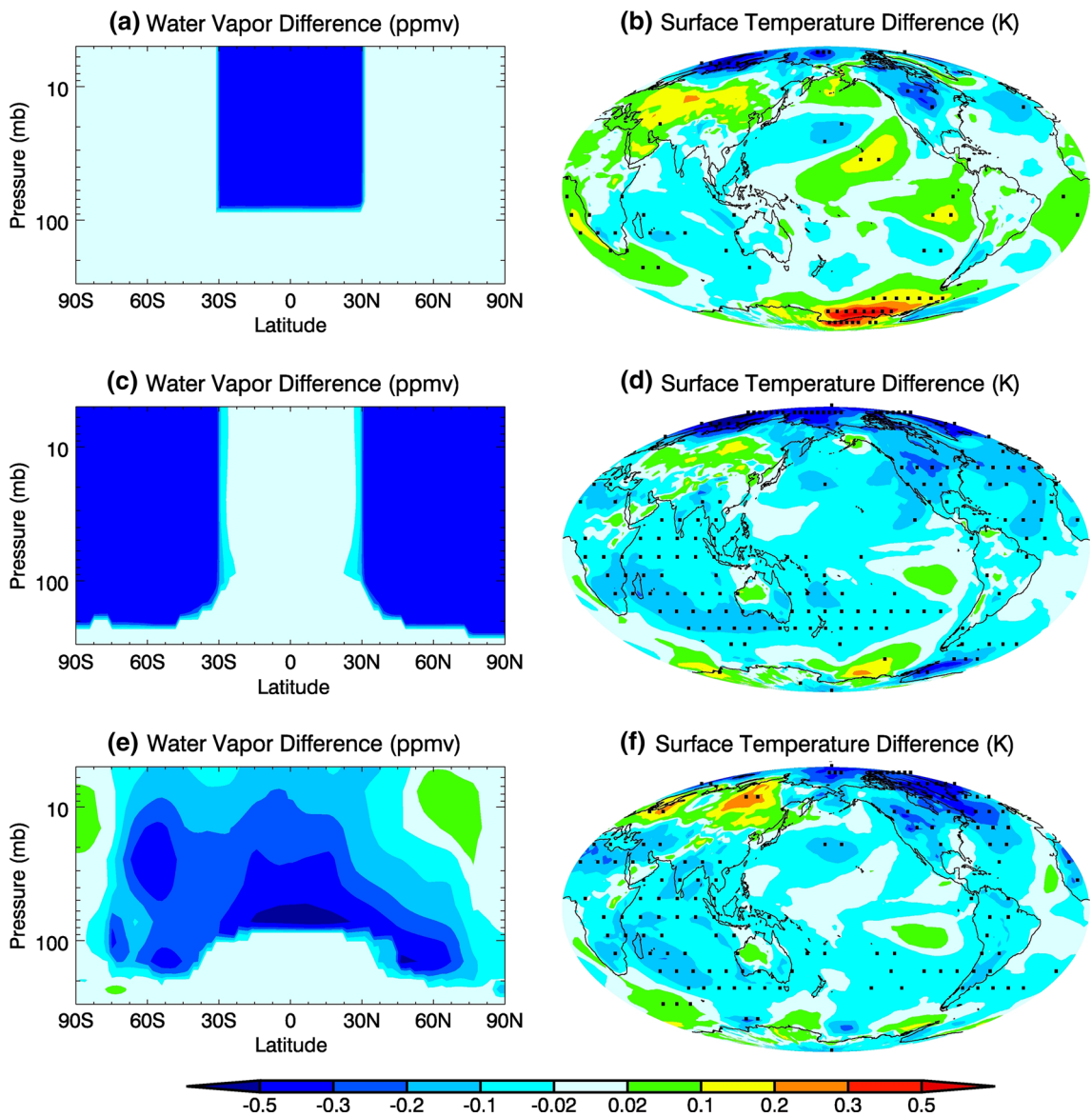


**Fig. 9** Left panels show SWV perturbations, with right panels showing the equilibrium surface temperature responses. **a** A uniform decrease of SWV by 0.5 ppmv only over the tropics (30°S–30°N). **b** The simulated ensemble-mean surface temperature difference between the control experiment and the sensitivity one with SWV

perturbations following (a). **c, d** Uniform decreases of SWV by 0.5 ppmv over the extratropics (90°S–30°S, 30°N–90°N) and associated responses. **e, f** Observed SWV decreases from 1997–2000 to 2001–2004 from GOZCARDS and associated responses

2010). The SWV forcing in the extratropics ( $-0.12 \text{ W/m}^2$ ) is about twice the tropical mean forcing ( $-0.064 \text{ W/m}^2$ ), in spite of the smaller SWV change over the extratropics than over the tropics (Fig. 9e).

### 3.2.3 Transient response to linearly increasing SWV

To investigate the transient response of surface temperature to time-varying SWV perturbations, we impose a linear trend in SWV based on satellite measurements. A positive linear trend of SWV is derived from GOZCARDS data

during 1992–2000 and 2004–2013. Averaging the trends over the two periods, we find a widespread moistening over most of the stratosphere (Fig. 10a). The most intense increases are located above the 20 hPa level in both hemispheres, while the SWV increase in the Southern Hemisphere is weaker than that in the Northern Hemisphere. In Exp. 7, CESM is forced by such a linearly increasing SWV for 50 years (Fig. 10b). We integrate the model over 50 years rather than a longer period in consideration of the fact that it is unlikely for SWV to keep steadily increasing without any interruption from one or more major drops for

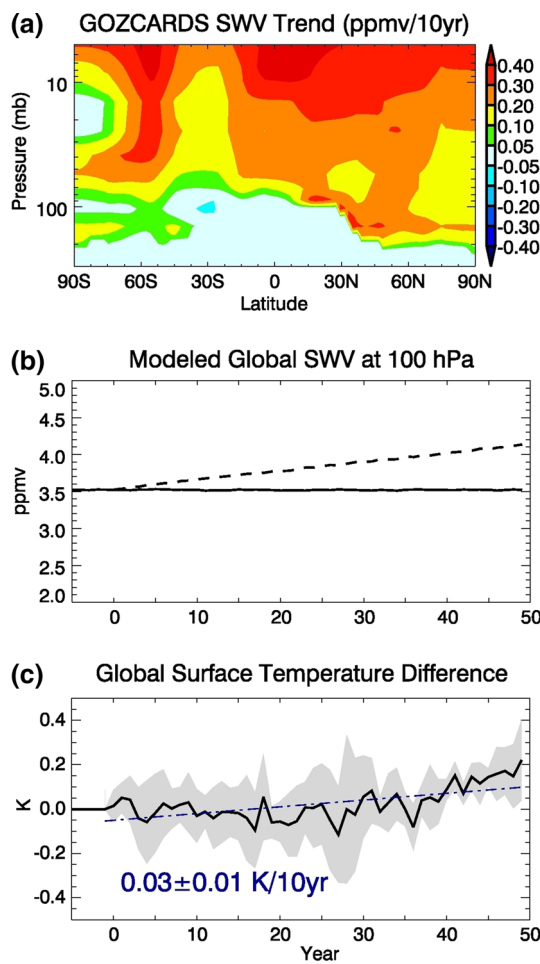


**Fig. 10** **a** Linearized SWV trends derived from the GOZCARDS record averaged over two intervals: 1992–2000 and 2004–2013. **b** SWV at 100 hPa in the control run (*solid line*) and sensitivity run (*dashed line*). **c** The simulated ensemble-mean surface temperature difference between the sensitivity test with SWV increasing at the rates in (a) and the control experiment. The *blue dash-dot line* is the linear regression of the temperature trend over 50 years. *Gray areas* indicate one standard deviation between ensemble members

more than 50 years. The ensemble-mean surface temperature from four member runs shows a  $0.032 \pm 0.013$  °C/decade surface warming in the global mean (Fig. 10c), corresponding to about  $19 \pm 7$  % of the observed global warming of 0.17 °C/decade from 1980 to 2000. The calculated warming rate from the transient experiments is lower than that from the simplistic estimation using the equilibrium response in Exp. 2, partially due to the smaller magnitude of the observed water vapor trends in the lower stratosphere during 1992–2000 and 2004–2013 than the previously reported 10 % per decade rate of SWV increase (Rosenlof et al. 2001).

The warming effect simulated by the CESM is only significant when considered over several decades. From Fig. 10c, it is clear that there are several discernible

**Table 2** Surface temperature ( $T_s$ ) trend analysis over different periods in Exp. 7

Years since SWV perturbation imposed	10	20	30	40	50
$T_s$ diff. trend (K/10 year)	0.0015	-0.024	-0.017	0.0041	0.032
SD of $T_s$ diff. (K)	0.12	0.13	0.15	0.14	0.13
SD of trend (K/10 year)	0.11	0.11	0.052	0.0081	0.013

$T_s$  diff. denotes the  $T_s$  difference between a control run and an experiment run with SWV perturbations. The standard deviation (SD) is the spread of the ensemble members relative to the ensemble mean

intervals of surface temperature decrease over the 50 years of simulations (year 0–5, 27–30, etc.), and the warming rate is not constant even though we have imposed a constant rate of increase in SWV. The last decade in Fig. 10c exhibits a much larger warming rate than previous decades. To better examine the model response as a function of analysis period length, we list the linearized trends and their spreads between different ensemble members analyzed over different periods in Table 2. It shows that the warming trend is only statistically significant when calculated over the whole 50-year period. Within the first 40 years, when the SWV increase is still less than 0.5 ppmv at 100 hPa (Fig. 10b), the SWV forcing is largely masked by the model internal variability, resulting in an insignificant response of surface temperature. Table 2 also shows that the spread of surface temperature response is generally reduced along with the time integration after 30 years. These results suggest that a linearly trending SWV forcing could not produce an instantaneously detectable signal in surface temperature, especially when the response to the prescribed forcing is insignificant compared to atmospheric internal variability. Therefore, the transient response in CESM to time-varying SWV forcings includes a multi-year adjustment before a persistent climate change signal stands out, given a moderate forcing magnitude. The time-scale for a significant surface temperature trend depends on the strength of the forcing relative to the internal variability of the climate system. A forcing of larger magnitude may enable a shorter detection period for the resulting surface temperature signal.

#### 4 Discussion and conclusions

We employ satellite water vapor observations and a coupled atmosphere–ocean general circulation model to investigate the relationship between SWV and surface temperature. The increasing trends of SWV from 1992–2000 to 2004–2013 as well as the SWV sudden drop after 2000 are clearly identified in the recently developed long-term GOZCARDS satellite record (Froidevaux et al.

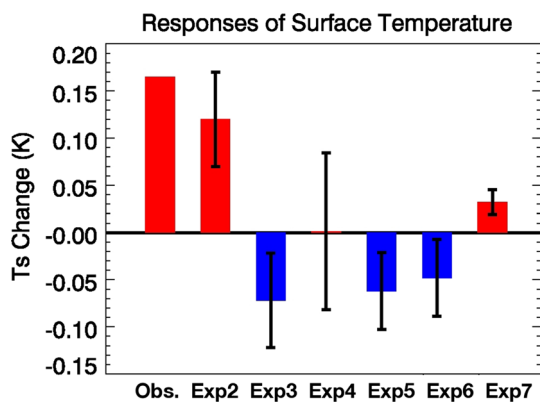


**Fig. 11** Summary of surface temperature responses from each experiment. ‘Obs.’ denotes the decadal mean temperature change over 1980–2000 from the CRU and GISS observational datasets. The decadal mean temperature change is shown from Exp. 7

2015). The NCAR CESM model was set up in different ways to assess the interactions between SWV and surface temperature.

First, an atmosphere-only model experiment driven by the interannual variations of the observed SST shows that the variations of tropical-mean water vapor in the lower stratosphere are highly correlated with the tropical-mean SST on the seasonal scale. This is consistent with previous studies showing that the interannual variations of SWV are partly driven by surface or tropospheric temperature (Dessler et al. 2013; Rosenlof and Reid 2008). However, after removing the seasonal cycle, the SWV and SST do not obey a simple correlation in the model fields, suggesting that the processes that govern the interannual variations of SWV are not limited to SST.

Treating SWV as an external forcing to the surface climate, we conduct a series of coupled atmosphere–ocean model experiments using a nudging approach to regulate the SWV amount (Fig. 11). A uniform increase in SWV of 1 ppmv in CESM produces a robust surface warming of about  $0.12^{\circ}\text{C}$  ( $\pm 0.05^{\circ}\text{C}$ ) in the global mean averaged over 50 years. On the other hand, a uniform decrease in SWV of 0.5 ppmv produces a surface cooling of  $-0.07^{\circ}\text{C}$  ( $\pm 0.05^{\circ}\text{C}$ ) in the global mean at equilibrium. Sensitivity experiments show that the response of global mean surface temperature to SWV perturbations over the extratropics is larger than that in response to the same amount of SWV perturbation over the tropics. The same  $-0.5$  ppmv SWV reduction confined to the extratropics (poleward of  $30^{\circ}\text{N/S}$ ) induces a  $-0.062^{\circ}\text{C}$  cooling globally, while SWV reductions limited to the tropics do not result in any significant cooling in global mean. Such a contrast indicates the importance of SWV variations at middle or high latitudes, and also underscores the importance of examining the spatial distributions of SWV variations when assessing

the SWV influence on global-mean surface temperature changes in future studies.

To evaluate the impact of observed increasing trends in SWV from 1992–2000 to 2004–2013, we impose a linearly increasing SWV amount based on the average of the SWV rates of change during those two periods in the multi-decadal model simulations. Our model yields a surface warming of about  $0.03 \pm 0.01^{\circ}\text{C}/\text{decade}$ , which is approximately 19 % of the observed rate of global warming before the warming hiatus (1980–2000). The warming trend is only statistically significant when calculated over the whole 50-year period, and the spread of surface temperature responses among the model ensemble members tends to decrease with integration time after 30 years. Such a transient response in CESM to the time-varying SWV forcing implies a multi-year adjustment period before a persistent climate change signal stands out, given a relatively weak SWV forcing initially. It is worthwhile to point out that the simulated response of the surface temperature depends on the magnitude of the observed linear trend in SWV. Since SWV exhibits large interannual variations, the linearized rates of change in SWV can be quite different for different analysis periods.

When driven by the SWV variation derived from satellite measurements, the surface temperature cooling concurrent with the sudden drop of SWV after 2000 is discernible in the model results. From our multi-decadal simulations, the equilibrium response of the surface temperature to the abrupt drop is about  $-0.048^{\circ}\text{C}$  ( $\pm 0.041^{\circ}\text{C}$ ), which approximately corresponds to one third of the global warming rate from 1980 to 2000. The associated forcing in the coupled model is consistent with the radiative model calculation [Solomon et al. 2010]. Therefore, our model shows that a persistent trend in SWV would undoubtedly make an imprint on long-term variations of global-mean surface temperature. The transient response to the sudden drop of SWV right after 2000 is rather uncertain based on additional experiments using CAM5-SOM and is not reported here, mainly because the response to the imposed forcing associated with the SWV drop is not strong enough to exceed the model internal variability within a short integration period. Only when the average over a long integration period is taken does the response become statistically significant compared to the muted background noise.

In general, the simulated equilibrium response of surface temperature to SWV perturbations from the coupled atmosphere–ocean models is comparable to that from simpler models such as the EMIC used by Solomon et al. (2010). Since the CESM model cannot resolve stratospheric dynamics such as wave drag, the SWV-induced changes in stratospheric circulation reported by Maycock et al. (2013) are absent in our simulations. Hence, the similarity between this model and the previous simple

models could be attributed to the weak circulation response in those models. Also note that the simulated responses of surface temperature to the observed SWV variations are subject to uncertainties arising from the satellite record as well as from model limitations. Considering the shortcomings of the slab ocean model in representing ocean dynamics, a fully coupled atmosphere–ocean simulation will be performed in a future study to assess the dependence of the modeled SWV influence on the sophistication of the atmosphere–ocean coupling. More ensemble members (ideally more than ten rather than the three or four used here) in future ensemble simulations are expected to reduce the sensitivity of our results to internal variability of the individual ensemble members.

**Acknowledgments** The authors thank Prof. Susan Solomon for helpful discussions. We appreciate the funding support by Aura MLS project, NASA ROSES10-COUND, ROSES12-MAP, ROSES13-NDOA and ROSES13-AST programs. The research was carried out at the Jet Propulsion Laboratory, California Institute of Technology, under a contract with NASA. The description of Global Ozone Chemistry And Related trace gas Data records for the Stratosphere can be found at <https://gozcards.jpl.nasa.gov/> and the related data distribution is through <http://mirador.gsfc.nasa.gov>; the GOZCARDS project was funded by NASA under the MEASUREs (Making Earth System Data Records for Use in Research Environments) program. The NCAR Community Earth System Model can be downloaded from <http://www2.cesm.ucar.edu/>. The surface temperature data from Climatic Research Unit can be obtained from <http://www.cru.uea.ac.uk/cru/data/temperature/>. The NASA GISS surface temperature data can be obtained at <http://data.giss.nasa.gov/gistemp/>.

## References

- Anderson J et al (2013) GOZCARDS merged data for water vapor monthly zonal means on a geodetic latitude and pressure grid V1.01 (GozMmlpH2O) at GES DISC, version 1.01, Greenbelt, MD, USA, NASA Goddard Earth Science Data and Information Services Center, Accessible at doi:[10.5067/MEASURES/GOZCARDS/DATA3004](https://doi.org/10.5067/MEASURES/GOZCARDS/DATA3004)
- Booth BBB, Dunstone NJ, Halloran PR, Andrews T, Bellouin N (2012) Aerosols implicated as a prime driver of twentieth-century North Atlantic climate variability 484, 228. *Nature* 485:534. doi:[10.1038/Nature11138](https://doi.org/10.1038/Nature11138)
- Castanheira JM, Peevey TR, Marques CAF, Olsen MA (2012) Relationships between Brewer–Dobson circulation, double tropopause, ozone and stratospheric water vapour. *Atmos Chem Phys* 12:10195–10208. doi:[10.5194/acp-12-10195-2012](https://doi.org/10.5194/acp-12-10195-2012)
- Chen X, Tung K-K (2014) Varying planetary heat sink led to global-warming slowdown and acceleration. *Science* 345:897–903. doi:[10.1126/science.1254937](https://doi.org/10.1126/science.1254937)
- Deser C, Phillips AS, Bourdette V, Teng H (2010) Uncertainty in climate change projections: the role of internal variability. *Clim Dyn* 38:527–546. doi:[10.1007/s00382-010-0977-x](https://doi.org/10.1007/s00382-010-0977-x)
- Dessler AE, Schoeberl MR, Wang T, Davis SM, Rosenlof KH (2013) Stratospheric water vapor feedback. *Proc Natl Acad Sci USA* 110:18087–18091. doi:[10.1073/Pnas.1310344110](https://doi.org/10.1073/Pnas.1310344110)
- Dessler AE, Schoeberl MR, Wang T, Davis SM, Rosenlof KH, Vernier JP (2014) Variations of stratospheric water vapor over the past three decades. *J Geophys Res Atmos* 119:12588–512598. doi:[10.1002/2014jd021712](https://doi.org/10.1002/2014jd021712)
- England MH et al (2014) Recent intensification of wind-driven circulation in the Pacific and the ongoing warming hiatus. *Nat Clim Change* 4:222–227. doi:[10.1038/NCLIMATE2106](https://doi.org/10.1038/NCLIMATE2106)
- Forster PMDF, Ponater M, Zhong W-Y (2001) Testing broadband radiation schemes for their ability to calculate the radiative forcing and temperature response to stratospheric water vapour and ozone changes. *Meteorol Z* 10:387–393. doi:[10.1127/0941-2948/2001/0010-0387](https://doi.org/10.1127/0941-2948/2001/0010-0387)
- Froidevaux L, Anderson J, Wang H-J, Fuller RA, Schwartz MJ, Santee ML, Livesey NJ, Pumphrey HC, Bernath PF, Russell JM III, McCormick MP (2015) Global ozone chemistry and related datasets for the stratosphere (GOZCARDS): methodology and sample results with a focus on HCl, H<sub>2</sub>O, and O<sub>3</sub>. *Atmos Chem Phys* 15:10471–10507. doi:[10.5194/acp-15-10471-2015](https://doi.org/10.5194/acp-15-10471-2015)
- Geoffroy O, Saint-Martin D, Olivie DJL, Volodire A, Bellon G, Tytca S (2013) Transient climate response in a two-layer energy-balance model. Part I: analytical solution and parameter calibration using AOGCM experiments. *J Clim* 26:1841–1857. doi:[10.1175/JCLI-D-12-00195.1](https://doi.org/10.1175/JCLI-D-12-00195.1)
- Gilford DM, Solomon S, Portmann RW (2016) Radiative impacts of the 2011 abrupt drops in water vapor and ozone in the tropical tropopause layer. *J Clim* 29:595–612. doi:[10.1175/JCLI-D-15-0167.1](https://doi.org/10.1175/JCLI-D-15-0167.1)
- Gregory J, Webb M (2008) Tropospheric adjustment induces a cloud component in CO<sub>2</sub> forcing. *J Clim* 21:58–71. doi:[10.1175/2007jcli1834.1](https://doi.org/10.1175/2007jcli1834.1)
- Hansen J, Sato M, Ruedy R (1997) Radiative forcing and climate response. *J Geophys Res-Atmos* 102:6831–6864. doi:[10.1029/96jd03436](https://doi.org/10.1029/96jd03436)
- Hansen J, Ruedy R, Sato M, Lo K (2010) Global surface temperature change. *Rev Geophys Artn.* doi:[10.1029/2010rg000345](https://doi.org/10.1029/2010rg000345)
- Hegglin MI et al (2014) Vertical structure of stratospheric water vapour trends derived from merged satellite data. *Nat Geosci* 7:768–776. doi:[10.1038/Ngeo2236](https://doi.org/10.1038/Ngeo2236)
- Held IM, Winton M, Takahashi K, Delworth T, Zeng FR, Vallis GK (2010) Probing the fast and slow components of global warming by returning abruptly to preindustrial forcing. *J Clim* 23:2418–2427. doi:[10.1175/2009jcli3466.1](https://doi.org/10.1175/2009jcli3466.1)
- Huang Y (2013) On the longwave climate feedbacks. *J Clim* 26:7603–7610. doi:[10.1175/JCLI-D-13-00025.1](https://doi.org/10.1175/JCLI-D-13-00025.1)
- Hurrell JW, Hack JJ, Shea D, Caron JM, Rosinski J (2008) A new sea surface temperature and sea ice boundary dataset for the Community Atmosphere Model. *J Clim* 21:5145–5153. doi:[10.1175/2008jcli2292.1](https://doi.org/10.1175/2008jcli2292.1)
- Hurrell JW et al (2013) The community earth system model a framework for collaborative research. *Bull Am Meteorol Soc* 94:1339–1360. doi:[10.1175/BAMS-D-12-00121.1](https://doi.org/10.1175/BAMS-D-12-00121.1)
- IPCC (2013) Climate change 2013: the physical science basis. Contribution of Working Group I to the Fifth Assessment Report of the Intergovernmental Panel on Climate Change. Cambridge University Press, Cambridge. doi:[10.1017/CBO9781107415324](https://doi.org/10.1017/CBO9781107415324)
- Jiang JH et al (2010) Five year (2004–2009) observations of upper tropospheric water vapor and cloud ice from MLS and comparisons with GEOS-5 analyses. *J Geophys Res-Atmos* 115:D15103. doi:[10.1029/2009jd013256](https://doi.org/10.1029/2009jd013256)
- Jiang JH et al (2012) Evaluation of cloud and water vapor simulations in CMIP5 climate models using NASA “A-Train” satellite observations. *J Geophys Res-Atmos.* doi:[10.1029/2011jd017237](https://doi.org/10.1029/2011jd017237)
- Jiang JH et al (2015) An assessment of upper-troposphere and lower-stratosphere water vapor in MERRA, MERRA2 and ECMWF reanalyses using Aura MLS observations. *J Geophys Res-Atmos* 120:11468–11485. doi:[10.1002/2015JD023752](https://doi.org/10.1002/2015JD023752)
- Kaufmann RK, Kauppi H, Mann ML, Stock JH (2011) Reconciling anthropogenic climate change with observed temperature 1998–2008. *Proc Natl Acad Sci USA* 108:11790–11793. doi:[10.1073/Pnas.1102467108](https://doi.org/10.1073/Pnas.1102467108)

- Kosaka Y, Xie SP (2013) Recent global-warming hiatus tied to equatorial Pacific surface cooling. *Nature* 501:403–407. doi:[10.1038/nature12534](https://doi.org/10.1038/nature12534)
- Liang CK, Eldering A, Gettelman A, Tian B, Wong S, Fetzer EJ, Liou KN (2011) Record of tropical interannual variability of temperature and water vapor from a combined AIRS-MLS data set. *J Geophys Res.* doi:[10.1029/2010jd014841](https://doi.org/10.1029/2010jd014841)
- Maycock AC, Shine KP (2012) Stratospheric water vapor and climate: sensitivity to the representation in radiation codes. *J Geophys Res-Atmos* 117:D13102. doi:[10.1029/2012jd017484](https://doi.org/10.1029/2012jd017484)
- Maycock AC, Joshi MM, Shine KP, Scaife AA (2013) The circulation response to idealized changes in stratospheric water vapor. *J Clim* 26:545–561. doi:[10.1175/jcli-d-12-00155.1](https://doi.org/10.1175/jcli-d-12-00155.1)
- Meehl GA, Collins WD, Boville BA, Kiehl JT, Wigley TML, Arblaster JM (2000) Response of the NCAR climate system model to increased CO<sub>2</sub> and the role of physical processes. *J Clim* 13:1879–1898. doi:[10.1175/1520-0442\(2000\)013<1879:Rotncs>2.0.Co;2](https://doi.org/10.1175/1520-0442(2000)013<1879:Rotncs>2.0.Co;2)
- Meehl GA, Arblaster JM, Fasullo JT, Hu AX, Trenberth KE (2011) Model-based evidence of deep-ocean heat uptake during surface-temperature hiatus periods. *Nat Clim Change* 1:360–364. doi:[10.1038/NCLIMATE1229](https://doi.org/10.1038/NCLIMATE1229)
- Morice CP, Kennedy JJ, Rayner NA, Jones PD (2012) Quantifying uncertainties in global and regional temperature change using an ensemble of observational estimates: the HadCRUT4 data set. *J Geophys Res-Atmos.* doi:[10.1029/2011jd017187](https://doi.org/10.1029/2011jd017187)
- Randel WJ, Wu F, Oltmans SJ, Rosenlof K, Nodolua GE (2004) Interannual changes of stratospheric water vapor and correlations with tropical tropopause temperatures. *J Atmos Sci* 61:2133–2148
- Randel WJ, Wu F, Vomel H, Nedoluha GE, Forster P (2006) Decreases in stratospheric water vapor after 2001: links to changes in the tropical tropopause and the Brewer–Dobson circulation. *J Geophys Res-Atmos* 111:D12312. doi:[10.1029/2005jd006744](https://doi.org/10.1029/2005jd006744)
- Reichler T, Dameris M, Sausen R (2003) Determining the tropopause height from gridded data. *Geophys Res Lett* 30:2042. doi:[10.1029/2003gl018240](https://doi.org/10.1029/2003gl018240)
- Richter JH, Solomon A, Bacmeister JT (2014) Effects of vertical resolution and nonorographic gravity wave drag on the simulated climate in the Community Atmosphere Model, version 5. *J Adv Model Earth Syst* 6:357–383. doi:[10.1002/2013MS000303](https://doi.org/10.1002/2013MS000303)
- Rosenlof KH, Reid GC (2008) Trends in the temperature and water vapor content of the tropical lower stratosphere: Sea surface connection. *J Geophys Res-Atmos.* doi:[10.1029/2007jd009109](https://doi.org/10.1029/2007jd009109)
- Rosenlof KH et al (2001) Stratospheric water vapor increases over the past half-century. *Geophys Res Lett* 28:1195–1198. doi:[10.1029/2000gl012502](https://doi.org/10.1029/2000gl012502)
- Soden BJ, Held IM (2006) An assessment of climate feedbacks in coupled ocean–atmosphere models. *J Clim* 19:3354–3360. doi:[10.1175/Jcli3799.1](https://doi.org/10.1175/Jcli3799.1)
- Solomon S, Rosenlof KH, Portmann RW, Daniel JS, Davis SM, Sanford TJ, Plattner GK (2010) Contributions of stratospheric water vapor to decadal changes in the rate of global warming. *Science* 327:1219–1223. doi:[10.1126/science.1182488](https://doi.org/10.1126/science.1182488)
- Su H, Waliser DE, Jiang JH, Li JL, Read WG, Waters JW, Tompkins AM (2006) Relationships of upper tropospheric water vapor, clouds and SST: MLS observations, ECMWF analyses and GCM simulations. *Geophys Res Lett.* doi:[10.1029/2006gl027582](https://doi.org/10.1029/2006gl027582)
- Takahashi H, Su H, Jiang JH (2015) Error analysis of upper tropospheric water vapor in CMIP5 models using “A-Train” satellite observations and reanalysis data. *Clim Dyn.* doi:[10.1007/s00382-015-2732-9](https://doi.org/10.1007/s00382-015-2732-9)
- Trenberth KE, Fasullo JT (2013) An apparent hiatus in global warming? *Earth’s Future* 1:19–32. doi:[10.1002/2013ef000165](https://doi.org/10.1002/2013ef000165)
- Urban J, Lossow S, Stiller G, Read WG (2014) Another drop in water vapor EOS. *Trans Am Geophys Union* 95:245–252
- Wang Y, Jiang J, Su H (2015) Atmospheric responses to the redistribution of anthropogenic aerosols. *J Geophys Res Atmos* 120:9625–9641. doi:[10.1002/2015JD023665](https://doi.org/10.1002/2015JD023665)
- Watanabe M, Shiogama H, Tatebe H, Hayashi M, Ishii M, Kimoto M (2014) Contribution of natural decadal variability to global warming acceleration and hiatus. *Nat Clim Change* 4:893–897. doi:[10.1038/NCLIMATE2355](https://doi.org/10.1038/NCLIMATE2355)
- Zhang K et al (2014) Technical note: on the use of nudging for aerosol–climate model intercomparison studies. *Atmos Chem Phys* 14:8631–8645. doi:[10.5194/acp-14-8631-2014](https://doi.org/10.5194/acp-14-8631-2014)